Comparing the catalytic activity of the water gas shift reaction on Cu(321) and Cu(111) surfaces: step sites do not always enhance the overall reactivity

Hèctor Prats, Pablo Gamallo, Francesc Illas, Ramón Sayós*

Departament de Ciència de Materials i Química Física & Institut de Química Teòrica i Computacional (IQTCUB), Universitat de Barcelona, C. Martí i Franquès 1, 08028 Barcelona, Spain.
** Corresponding author: Ramón Sayós*
Email: r.sayos@ub.edu / Tel. +34934034760

Abstract

A Density Functional Theory based first-principles kinetic Monte Carlo (kMC) study of the water gas shift reaction on the stepped Cu(321) surface is presented. We use the recently developed graph-theoretical kMC approach coupled with cluster expansion Hamiltonians to model the coverage-dependent energy barriers for the different surface processes, including adsorption/desorption, diffusion and other elementary chemical reactions, totalling 36 elementary steps, which allow two possible competitive mechanisms: surface redox and associative COOH. All results are compared to a previous kMC study on Cu(111). Both mechanisms are observed for Cu(321) surface with different extension, whereas the associative COOH one was the dominant for Cu(111). The present study shows that, in spite of encompassing lower activation energy barriers, stepped surfaces do not necessarily have an overall larger catalytic activity. Coverage effects and the significant contribution of some of the reverse processes are behind this behaviour.

Keywords

Kinetic Monte Carlo, water gas shift reaction, copper (321) surface, density functional theory, associative COOH mechanism, surface redox mechanism, rate-determining step, catalytic activity

1. Introduction

Low coordinated sites play an important role in many heterogeneously catalysed reactions [1-3]. In particular, step sites are often crucial since, for instance, they allow different types of binding to the catalyst surface [4], and facilitate bond breaking of reactants [5]. It is generally assumed that the presence of steps enhances the catalytic activity towards a complex reaction by increasing the reactants adsorption energies and decreasing the energy barriers as shown by Honkala *et al*. [6] for the case of NH_3 synthesis over models of a Ru catalyst. However, even if the energy barriers for the rate-determining steps (RDS) at step sites are lower than for regular sites, it is not always possible to conclude that the presence of these sites is beneficial. In fact, a strong chemisorption of reactants, products or impurities may cause surface poisoning [7], and may also result in the lowering of the energy barriers for RDSs also in the reverse direction, increasing reverse reaction rates over the forward ones with a concomitant decrease of the catalytic activity.

An important catalysed reaction with special technological relevance [8] is the water gas shift reaction (WGSR) that transforms CO and H_2O into CO_2 and H_2. It is an equilibrium-limited reaction, where CO conversion is favoured at low temperatures due to its exergonicity (*i.e.*, $\Delta_r G^0_{298.15K}$ = - 0.30 eV). As the temperature increases, the equilibrium constant and the final conversion inherently decrease. Hence, this process is usually carried out in two stages: a first one at quite high temperature (300-450 ºC) favouring fast CO consumption, and a second one at a lower temperature (200-300 ºC) to reach higher conversions, which are limited by the thermodynamic equilibrium [9]. Copper based catalysts with inclusion of Zn, Cr and Al oxides [10] and $CuO/ZnO/Al_2O_3$ [11] are used in low temperature reactors [12], although other metals and supports have also been proposed [13,14].

The molecular mechanism for the low temperature catalysed WGSR involves a rather large number of elementary steps defining the two possible main routes, usually referred to as surface redox and associative COOH mechanisms [15]. Both start from H_2O dissociation, however in the former CO_2 is produced by direct reaction between adsorbed CO and O, whereas in the latter it is generated through a COOH intermediate.

Following the initial work of Fajin *et al.* [16], we have recently studied the role of step sites in the WGSR catalysed by Cu surfaces using Density Functional Theory (DFT) calculations including the contribution of dispersion terms [17]. Thus, we compared the energy barriers for all the different pathways involved in the two molecular routes for both the stepped Cu(321) surface and the flat Cu(111) one [18]. Although the presence of step sites increases the water adsorption energy and decreases the energy barriers of different processes (*e.g.*, the water dissociation and CO_2 formation from CO oxidation, among others) one cannot rigorously claim that the catalytic activity of the stepped surface is going to be superior to that of the flat Cu(111) surface, where the COOH formation is faster and the water formation (*i.e.,* the rate-determining step in the reverse direction) has an energy barrier much higher than on the stepped Cu(321) surface [17]. In fact, some previous studies, for instance, for the reverse WGSR [19] and for the WGSR [20] on Cu(hkl) surfaces conclude that catalytic activity follows the order Cu(110) > Cu(100) > Cu(111). However, these claims are based on comparing only energy barriers of some assumed RDSs. Note that the use of rate constants would include at least entropic and temperature effects. Clearly, a more rigorous approach would imply to introduce temperature, pressure, reverse processes and surface coverage effects on the overall reaction, which also would allow a much better estimate of the RDSs. This can be done by using either microkinetic modelling or kMC simulations. Usually, the RDS for the same global reaction involving a complex mechanism, as the case of the WGSR, can depend on the type of catalytic surface along with the T and P conditions [21]. Within a microkinetic model, a rather rigorous determination of a RDS (often several ones) can be done through the evaluation of the degree of rate control for the proposed step as defined by Campbell [22], or by doing a most sophisticated reaction-route graph analysis based on an equivalent electrical circuit [21,23]. Another similar methods are also available [24, 25].

In the current study, we present kinetic Monte Carlo simulations of the WGSR over the Cu(321) surface, based on earlier DFT calculations [17], to ascertain its catalytic activity in comparison to a previous kMC study over the flat Cu(111) surface [18]. Moreover, we apply the Campbell's degree of rate control in kMC simulations in an attempt to accurately establish the main RDSs, also applied in a previous [26]. By comparing the Campbell factors obtained with the analysis of the different frequencies of

the main elementary processes involved in the WGSR mechanism, we provide compelling evidence of the usefulness of this important concept in kMC simulations and its general validity beyond microkinetics models.

2. Computational methods

2.1 DFT calculations

The optimized geometries, energy barriers and the corresponding vibrational frequencies for the reactants, products and transition states involved in the different reaction pathways of the WGSR over the Cu(321)-stepped surface have been computed and characterized at DFT level in a previous study, using a standard generalized gradient approximation (GGA) type functional and accounting explicitly for dispersion terms [17], as explained in detail below. Moreover, we have performed additional DFT calculations in order to obtain the corresponding diffusion barriers of those species that could diffuse easily over the surface, as well as to determine the main lateral interactions between the different coadsorbed reactant pairs.

All periodic DFT calculations in the present work were performed by means of VASP code [27-29]. The slab was modelled through a 2×2×1 supercell constructed using the optimum lattice parameter of 3.63 Å (experimental value 3.62 Å [30]). The GGA type DFT calculations were carried out with the PBE functional [31]. The effect of van der Waals interactions was included by adding the dispersion term obtained from the D2 method of Grimme [32] to the PBE calculated energy (PBE-D2) as in our previous work [17]. The valence electron density was expanded in a plane-wave basis set with a cut-off of 415 eV for the kinetic energy. The effect of core electrons in the valence electron density was taken into account using the projector augmented wave (PAW) method [33] as implemented in the VASP code [34]. Numerical integration in the reciprocal space was carried out by employing a 5×5×1 Monkhorst-Pack grid of special *k*-points [35]. The convergence thresholds were 10^{-6} eV for the total energy and 10^{-3} eV•Å^{-1} for the forces acting on the cores. Additional details about the periodic DFT calculations are reported in our previous work [17].

2.2 kMC simulations

We use the full set of DFT data described above to perform kMC simulations at the molecular level. The coupling of kMC with DFT calculations renders the simulation a truly first-principles approach. From an efficiency perspective, kMC can simulate reactions with a computational expense that is much lower than that needed for ab initio molecular dynamics, and represents an improvement compared to the existing mean-field microkinetic models that, among other issues, cannot take into account the detailed structure of stepped surfaces such as the Cu(321).

The kMC method simulates the time evolution of a system at the molecular level, in which all the possible reactions or processes that can occur have an associated reaction rate [36]. In the present study, we use the recently developed graph-theoretical kMC approach [37] coupled with cluster expansion (CE) Hamiltonians [38,39] for the adlayer energetics by means of ZACROS code [37,38]. As in previous kMC schemes, a simulation is initialized with a given lattice configuration (in our case an empty lattice), and a list is generated containing all the possible lattice processes for the given configuration. Then, the algorithm enters a loop where, at each step, the most imminent process in the queue is executed (*i.e.*, the one with the smallest time of occurrence according to the first-reaction method [40]), until the stop conditions are fulfilled. Finally, a stochastic trajectory is obtained containing all the information about the lattice configuration as well as the number of gas-phase molecules produced or consumed at every time step. This trajectory can be analysed to get information such as the equilibrium surface coverage, the final CO_2 and/or H_2 production or the contribution of each possible reaction channel.

2.2.1 Lattice-gas model

The Cu(321)-stepped surface has different low-coordinated atoms and includes a high heterogeneity of adsorption sites such as terraces, nearby kinks and steps. Although it is less stable than the Cu(111) or Cu(100) low Miller index surfaces, its study is interesting to better understand the grounds of the catalytic activity and the contribution of the featured sites likely to be present in a real polycrystalline catalyst, formed by several facets. We

distinguish five different top sites (named 1, 2, 3, 4 and 5) and six different hollow sites (named *a*, *b*, *c*, *d*, *e* and *f*). Moreover, a molecule adsorbed in a bridge position between top sites *i* and *j* is labelled as $b_{i\text{-}j}$. Fig. 1 shows the location of those sites over the surface.

In order to carry out the kMC simulations, a suitable model of the surface is needed. In the present work, the Cu(321) surface is represented by a two-dimensional periodic grid of points, where each point represents one catalytically active surface site. For simplicity, only top sites are explicitly defined in our lattice model. In that way, a molecule adsorbed in a bridge site $b_{i\text{-}j}$ is labelled as occupying two neighbouring *top i* and *top j* sites. In an equivalent manner, molecules adsorbed on hollow sites (*i.e.*, H and OH) involve some of the surrounding top sites (see Section II in the Supplementary Information for more details). *Top 5* sites are located at the bottom of the step, a region displaying a large Pauli (steric) repulsion. Thus, they have not been included in the lattice model because adsorption at these sites is very improbable. Accordingly, the model unit cell has a total of 4 top sites (*i.e.*, *top 1*, *top 2*, *top 3* and *top 4*). Note that even though all lattice sites in the grid are on a plane, the real surface is not planar (Fig. 1) and the difference in bonding at the different sites is accounted for in the DFT calculated data serving as input for the kMC simulations.

The convergence of kMC simulations with respect to the lattice size has been tested by computing the final (*i.e.*, steady-state) H_2 production for several surface models with different $L \times L$ number of unit cells in the range $5 \leq L \leq 40$, concluding that the results for the *10×10* lattice model (including a total of 400 sites) virtually coincide with those obtained using larger surface models.

2.2.2 Reaction network

A full set of 36 elementary processes were considered for the molecular mechanism of the WGSR, which are described in Table 1, where "+" and "-" signs stand for forward and reverse processes, respectively (schemes of the energy profiles for most of the processes are reported in Section I of the Supplementary Information). These processes include the most important elementary steps, previously characterized by using DFT calculations [17], but adding also 14 new possible diffusion processes for H, O and OH. In this study, the adsorption of CO molecules is restricted to the step sites (*i.e.*, *top* 1) because

of the higher binding energy compared to the other top sites (*i.e.*, around 0.60 eV larger); thus, diffusion of CO molecules to the other top sites has not been included. In spite of the present network includes only the most favourable reaction pathways, involving a given selection of sites, the numerous diffusion processes available in kMC simulations allow adsorbed species to reach the most stable configurations and then evolves through the processes considered in the present network.

In the graph-theoretical kMC approach, each elementary step is represented as a graph pattern, with specific initial and final states. This choice enables the representation of complex elementary steps involving multidentate adsorbates in specific binding configurations and neighbouring patterns. This approach has been used recently (without coupling with cluster expansion Hamiltonians) by Stamatakis *et al.* to investigate the WGSR on platinum surfaces [41].

In order to "translate" an elementary step into ZACROS's input, it is instructive to make use of drawings like the one sketched in Fig. 2. There, for instance, an adsorbed H in hollow "a" site is labelled as occupying *top 2* and *top 3* sites; and an adsorbed *c*-COOH in a bridge $b_{1\text{-}2}$ site is labelled as occupying *top 1* and *top 2* sites. Section III of the Supplementary Information contains the schematic drawings for all reaction steps. Note that all steps are reversible excepting CO_2 and H_2 desorption.

2.2.3 Reaction rates

The reaction rate of a surface elementary process, defined as the number of times this process occurs per site and time unit, can be calculated by using either the transition state theory (TST) or the collision theory (CT) [40, 42]. For a surface Langmuir-Hinshelwood type reaction, a desorption process or an atomic or molecular diffusion process, the reaction rate can be calculated as

$$r_i = \frac{k_B \cdot T}{h} \frac{Q_i^{\neq}}{Q_R} exp\left(-\frac{E_i^0(\sigma)}{k_B \cdot T}\right) \quad (1)$$

where h denotes Planck's constant, k_B the Boltzmann's constant, and $Q_i^{\neq}$ and Q_R are the partition functions (dimensionless) of the transition state and the reactants, respectively, which are calculated from standard statistical mechanical expressions [43]. Finally, $E_i^0(\sigma)$

stands for the coverage-dependent energy barrier for the i^{th} process, including the zero-point energy (ZPE) correction. In order to quantitatively model the configuration-dependent energetics, the formulation of CEs expands the energy of a configuration of adsorbates σ as as a sum of cluster energies [44 -48]:

$$H(\sigma) = \sum_{k=1}^{N_C} \frac{ECI_k}{GM_k} \cdot NCE_k(\sigma) \tag{2}$$

where $H(\sigma)$ is the Hamiltonian of the system (*i.e.*, energy of a lattice configuration); N_C is the total number of figures/clusters specified in the energetic model; ECI_k is the effective cluster energy of figure k; GM_k is the graph-multiplicity of that figure (*i.e.*, to avoid overcounting contributions, equivalent to a symmetry number); and NCE_k is the number of times that pattern of figure k appears in the lattice. Then, the reaction energy for i^{th} process is given as in equation (3), which follows the formulation of Nielsen et al. [38]

$$\Delta E_i(\sigma) = H(\sigma') - H(\sigma) + \Delta E_i^{gas} \tag{3}$$

where σ and σ' refer to the initial and final configurations of the overall lattice, respectively, and ΔE_i^{gas} is the change in the energy of gas species whenever they are involved in the process (*i.e.*, $E_{i,prod}^{gas} - E_{i,reac}^{gas}$). Microscopic reversibility dictates that the difference between forward and reverse energy barriers is equal to the reaction energy

$$\Delta E_i(\sigma) = E_{fwd,i}^0(\sigma) - E_{rev,i}^0(\sigma) \tag{4}$$

In the above expression, $\Delta E_i(\sigma)$ can be calculated from the CE Hamiltonian. The forward energy barrier can be parameterized in terms of a Brønsted–Evans–Polanyi (BEP) relationship [49,50]

$$E_{fwd,i}^0(\sigma) = max\left(0, \Delta E_i(\sigma), E_{fwd,i}^0(0) + \omega\big(\Delta E_i(\sigma) - \Delta E_i(0)\big)\right) \tag{5}$$

where the max operator filters negative values, as well as values lesser than $\Delta E_i(\sigma)$, if the latter is positive. Moreover, $E_{fwd,i}^0(0)$ and $\Delta E_i(0)$ are the energy barriers and reaction energies at the zero-coverage limit (*i.e.*, only reactants existing on the surface), and ω is the so-called proximity factor [51] ranging from 0.0 for a reactants-like transition state, to 1.0 for a products-like transition state. In that way, selecting ω = 0 keeps the forward barrier fixed at the zero-coverage limit DFT value and the reverse barrier is chosen to be thermodynamically consistent, whereas in the limit ω = 1 the reverse barrier is fixed to the DFT value and the forward one is adjusted. Assuming that the transition states can have

both reactant and product state characters, we assume ω = 0.5 for all elementary steps. The reverse energy barrier is then

$$E_{rev,i}^{0}(\sigma) = max\left(0, -\Delta E_i(\sigma), E_{rev,i}^{0}(0) - (1-\omega)\cdot\left(\Delta E_i(\sigma) - \Delta E_i(0)\right)\right) \quad (6)$$

where

$$E_{rev,i}^{0}(0) = E_{fwd,i}^{0}(0) - \Delta E_i(0) \quad (7)$$

Unlike other kMC studies for simpler systems like NO oxidation on Pt(111) [48] or CO oxidation on Pd(111) [52], where CE was used in order to fit a data set of 50 and 92 DFT calculations for different surface configurations, respectively, our parameters are fitted in order to reproduce properly both the energy profile for reactants at infinite separation and coadsorbed states for all the elementary steps of the WGSR mechanism (Table 1), including lateral interactions for all reactant and product pairs (i.e., 15 cases). Although this alternative is not as accurate as the one used in the above mentioned studies, it represents a step forward compared to the traditional kMC simulations, where only one energy barrier is used for each process. This fact is especially important for a correct description of the diffusion processes, where the energy barriers strongly depend on the local environment. As an example, consider the diffusion process of a single O atom moving from hollow "b" to hollow "a" site (*i.e.*, process -14a); if the O atom has no neighbours neither at the initial nor at the final state, its energy barrier will be 0.44 eV (*i.e.*, zero-coverage limit, see Table 1). However, if it is initially coadsorbed next to a H_2O molecule, the energy barrier for that process will be larger (*i.e.*, 0.59 eV, Eq. 5). Section IV on the Supplementary Information shows the graph patterns for all the figures/clusters included in the CE Hamiltonian and used in our calculations as input.

Due to the high number of species and site types present in the WGSR on Cu(321), it is impossible to fit a complete data set of DFT energies for all possible lateral interactions, which could appear through the reaction (i.e., at higher coverages), like was done in other but simpler works mentioned above. Thus, lateral interactions for non-reactant pairs (e.g., H_2O and OH) were not considered in the present study, like neither were included for Cu(111) previous study [18].

The rate of adsorption processes is given by the well-known Hertz-Knudsen equation as

$$r_i^{ad} = S_{0,i} \cdot A_{site} \cdot \frac{p_i}{\sqrt{2\pi m_i k_B T}} \quad (8)$$

where $S_{0,i}$ stands for the initial sticking coefficient, A_{site} correspond to the area of a single site, p_i is the gas partial pressure and m_i is the mass of the gas molecule. In the present study $S_{0,i}$ is taken as the unity for both gas reactants, as in previous studies over the Cu(111) surface [18,53,54].

In the current system, diffusion processes have energy barriers substantially lower than those corresponding to other elementary chemical reactions (Table 1). Consequently, in practice, most kMC steps in the simulation would correspond to diffusion processes with a small number of them corresponding to the chemical processes of interest. This fact implies that very large simulations would be required to obtain meaningful results. Thus, we have artificially reduced the diffusion rates of the fastest processes (*i.e.*, steps ±13b, ±15a and ±15c from Table 1) by three orders of magnitude. A sufficiently large number of additional simulations have been performed to check that this scaling factor speeds up the overall study without affecting the results. This approach has been also applied in previous kMC studies of WGSR over Cu(111) [18,55] leading to negligible errors in the different calculated properties [56].

3. Results and discussion

For the present kMC simulations the initial conditions correspond to an experiment with a fresh reactants mixture of CO and H_2O with P_{CO} and P_{H2O} partial pressures, continuously impinging on an empty thermalized Cu(321) surface, where the heterogeneous reaction takes place and afterwards the final gas products (*i.e.*, CO_2 and H_2) desorb and leave the surface region (*i.e.*, in a nonequilibrium thermodynamic state). The partial pressure and temperature values have been chosen to allow a direct comparison between the flat Cu(111) and the stepped Cu(321) surfaces. Each kMC simulation was allowed to achieve a steady-state in which surface coverage for all intermediates remains constant in time, with the exception of small fluctuations resulting from the stochastic nature of the method. From that point, the overall macroscopic kinetic properties were calculated, such as the turnover frequency (TOF), defined as the number of product species

formed per area and unit time (*i.e.*, $s^{-1} \cdot cm^{-2}$). The total number of kMC steps performed depends on the reaction temperature, ranging from 10^9 to 10^{10} kMC steps at T = 625 K and 463 K, respectively.

We also made an estimate of the effect of missing some lateral interactions for non-reactant pairs in our reaction network. Thus, for the H_2O/OH interactions, we carried out new DFT calculations to determine this kind of interactions (the 5 most favourable configurations were included in kMC simulations at 625 K with P_{CO} = 26 Torr and P_{H2O} = 10 Torr) and we observed that there was only a small decrease of the TOF (the log [TOF] passed from 17.47 to 17.35) and an increase of only the water coverage (passed from 7% to 14%), but these changes do not affect the comparison of the Cu(321) vs. Cu(111) WGSR activities.

3.1 Temperature effects

Plotting the logarithm of the computed H_2 TOF as a function of 1000/T leads to an Arrhenius behaviour in two temperature intervals, with apparent activation energies of 1.2 eV (550-625 K) and 1.6 eV (463-550 K, see Fig. 3). Noticeably, these values are higher than those corresponding to the flat Cu(111) surface (*i.e.*, E_a = 0.5-0.8 eV [18]), but the plots exhibit a similar shape. Moreover, within the 463-625 K temperature range, the TOF for the overall reaction at the stepped Cu(321) surface is between two (at 625 K) and four (at 463 K) orders of magnitude lower than when it takes place at the Cu(111) surface. It is important to mention that, despite the high number of elementary processes involved, the stoichiometry of the global reaction is preserved, except for the first simulation steps, where the $H_{2(g)}$ production is faster than the $CO_{2(g)}$ production.

For P_{CO} = 26 Torr and P_{H2O} = 10 Torr, Fig. 4 shows that adsorbed OH is the most dominant species at the surface in all the temperature range, followed by CO, H_2O and finally atomic H. On the contrary, at the Cu(111) surface, the H coverage presents the largest value, excepting at the highest temperature where OH also becomes the dominant surface species (*e.g.*, $\theta_H > \theta_{OH} > \theta_{H2O} > \theta_{CO}$ at 550 K). Another striking difference respect the Cu(111) surface is that the coverage of the different species at the Cu(321) surface is much less temperature-dependent, with the exception of H coverage, which decreases with

increasing temperature as on the flat surface. Note that the coverage of carboxyl species and atomic O is almost insignificant, because these species are very reactive.

Regarding the reaction mechanism, the associative COOH route (*i.e.*, processes 9, 10 and 11) is the dominant pathway in all the studied conditions (Fig. 5a), even when we change the ratio of partial pressures for both reactants. This point is in agreement with previous observations using mean-field microkinetic modelling [15] and kMC simulations [18] for the flat Cu(111) surface. However, at the Cu(321) surface, the surface redox route (*i.e.*, processes 6, 7 and 8), which does not play any role in the flat surface, becomes also important at high temperatures, contributing around a 12% of the overall TOF. On the flat Cu(111) surface, this process is severely hindered, because when atomic O is formed by process +7 it rapidly goes towards the opposite direction forming OH again since the forward process is highly endoergic and exhibits a very low energy barrier in the reverse direction. Nevertheless, on the stepped surface process +7 is more favoured since it is practically isoergic and the probability that a CO molecule finds an atomic O becomes greater.

Looking at the associative COOH route in some more detail, one finds that the energy barrier for direct carboxyl dehydrogenation (*i.e.*, process +10) on the Cu(111) surface is 1.18 eV, considerably higher than on the Cu(321) surface, where its value at zero-coverage limit is 0.80 eV. This fact causes that this process is not observed in the flat surface, but instead, is one of the main routes for CO_2 production on the stepped surface (Fig. 5a). On the other hand, the energy barrier for carboxyl disproportionation by hydroxyl (*i.e.*, process +11) is much lower compared to the direct carboxyl dehydrogenation for both surfaces (*i.e.*, 0.38 eV and 0.25 eV in Cu(111) and Cu(321), respectively). Nevertheless, on the Cu(321) surface both processes happen in a similar proportion. This is because carboxyl disproportionation by hydroxyl requires that a neighbouring OH reaches a $b_{1\text{-}4}$ position and this adsorbed species is usually located at hollow "a" or $b_{1\text{-}2}$ sites (see the diffusion energy profile in Section I of the Supplementary Information). Moreover, the direct carboxyl dehydrogenation is unimolecular.

The statistics of the most important elementary steps at low and high temperature for the reaction on Cu(321) are shown in Fig. 5b. In this figure, each pair of bars represents the event frequency per second and cm^2 for the forward (red) and reverse (blue) elementary

reactions. It is worth noting that the CO and H_2O adsorption/desorption are partially equilibrated reactions, along with water dissociation, OH disproportionation and carboxyl formation; all other elementary reactions are practically irreversible. In contrast, on the Cu(111) surface only reactants adsorption/desorption and OH disproportionation processes were found to be partially equilibrated. The RDSs at both temperatures appear to be the formation of CO_2 through the associative COOH route (*i.e.*, process +10 at low temperatures and process +11 at high temperatures), since these are the first steps in the sequence that are not partially equilibrated, and the TOF for these steps is several orders of magnitude lower than for the previous steps. This finding is contrary to the prediction by Fajin *et al*., based purely on energy profiles obtained from DFT calculations, that the RDSs on the Cu(321) surface should be the water dissociation and the hydrogen recombination [16]. Interestingly enough, the RDS found in the present work were also suggested by Grabow *et al.* in a previous microkinetic model of the WGSR over Pt(111) [51]. In spite of the fact that processes +10 and +11 do not present a very high energy barrier, they cannot compete against the carboxyl dissociation (*i.e.*, process -9), which has an energy barrier at zero-coverage limit of only 0.24 eV and it is specially favoured at high temperatures due to its endoergicity. The observed change in the slope of the Arrhenius plots for the two surfaces (Fig. 3) suggests that the RDS can vary with temperature (*i.e.*, process +10 at low temperature and process +11 at high temperature, or vice versa).

The statistical analysis of Fig. 5b also shows that at 500 K, one water molecule dissociates on average for every 10 water molecules adsorption, whereas at 625 K the ratio is increased to 1:2 (the water dissociation process is endoergic, being more favoured at high temperature). This feature enhances the frequency of OH recombination (*i.e*, process +7), producing more atomic oxygen and thus promoting the surface redox mechanism, which is negligible at low temperatures (Fig. 5a).

At this point, one may wonder why the computed H_2 TOF for the Cu(321) surface, where three different processes for CO_2 formation are participating, is lower than for the Cu(111) surface, where direct carboxyl dehydrogenation and CO oxidation do not occur. The reason is very simple. On the one hand, carboxyl formation (*i.e.*, process +9) is endoergic by 0.62 eV on the stepped surface, whereas on the flat surface becomes endoergic by only 0.15 eV. This change implies that the energy barrier in the reverse

direction is much lower in the stepped surface (*i.e.*, 0.24 eV) than in the Cu(111) surface (*i.e.*, 0.55 eV). On the other hand, something similar happens with water dissociation: whereas in the flat surface this process is exoergic and has an energy barrier of 1.15 eV in the reverse direction, it is endoergic in the stepped surface, with an energy barrier of 0.60 eV for the reverse direction (*i.e.*, the equilibrium constant for the stepped surface at 625 K is only 5.90×10^{-3}). Moreover, the poisoning of top 1 step sites by CO and, to a lesser extent, by water, prevents some elementary reactions to occur: this is the case for carboxyl disproportionation or H_2 formation (*i.e.*, within all the temperature range considered, the sum of H_2O and CO coverage is around 19-24%, which means that the percentage of occupied top 1 sites is between 76-96%, and only the remaining free sites may be available for other reactions). In fact, the lower H_2 production rate on Pt(211) compared to Pt(111) reported in the work of Stamatakis *et al*. [41] was attributed to the same effect.

The present results confirm that the catalytic activity of surfaces containing low-coordinated sites is not always higher, even if they present higher adsorption energies for reactants or lower energy barriers for the main elementary steps. Therefore, establishing a ranking of the most efficient crystal surfaces for catalysing a complex reaction (*e.g.*, WGSR) based only on the energy barriers of forward processes is not always correct, although this is often done [20,57,58]. Moreover, the RDSs may change from one catalyst to another, and these steps may not coincide with the processes having the highest energy barriers, as checked by performing kMC simulations or microkinetic modelling.

As an additional corroboration of the observed RDSs for the WGSR on Cu(321), derived from the analysis of the frequencies of all steps, we have investigated whether the Campbell's degree of rate control [22] (*i.e.*, $X_{rc,i}$ for step i), applied earlier and extensively in microkinetic modelling studies, could also be valid for kMC simulations, where there is an earlier similar study for CO oxidation at RuO_2(110) surface [26]. This parameter, mainly intended for kinetics where a steady-state or quasi-steady state rate are achieved, should take significant but less than 1 values for RDSs and negligible values for other steps. Table 2 shows calculated $X_{rc,i}$ values for four processes at several temperatures and partial pressures. Results in Table 2 show that processes +10 and +11 are clearly the RDSs for partial pressures of 26 and 10 Torr for CO and H_2O, respectively. This is in agreement with the results derived from the analysis of the frequencies of the steps. The increase of

temperature also indicates a change in the relative importance of both elementary steps, although contrary to the previous trend. Another important conclusion is that neither water dissociation (RDS for WGSR on Cu(111)) nor H recombination are RDSs for these conditions.

3.2 Pressure effects

The effects of reactants mixture composition on the overall H_2 TOF have been examined carrying out a series of kMC simulations with different H_2O/CO ratios ranging from 0.11 to 9.0 for a total pressure of 100 Torr and a reaction temperature of 625 K (Fig. 6). The RDSs for all these reactant mixtures are still the formation of CO_2 through the carboxyl intermediate, being processes +10 and +11 equally likely. Campbell's degree of rate control (Table 2) corroborates this conclusion, although process +11 is more important as RDS for P_{H2O}/P_{CO} = 10/90 Torr and process +10 for P_{H2O}/P_{CO} = 90/10 Torr. Thus, the associative COOH mechanism seems to be again the dominant reaction pathway. In spite of that, changes in the partial pressures increase also somewhat the importance of water dissociation or H recombination.

The maximum H_2 TOF corresponds to a H_2O/CO ratio between 0.25-0.40, slightly lower than for the Cu(111) surface, where the optimum value is between 0.43-0.66 [18]. This result can be explained by examining the coverage of the different adsorbates as a function of reactants partial pressures (Fig. 6a) and the frequencies of the main elementary processes for H_2O/CO ratios of 10/90 and 90/10 (Fig. 6b). As discussed in the previous section, carboxyl formation is a very endoergic process, with a small equilibrium constant of 2.50×10^{-5} at 625 K. This value implies that a high concentration of adsorbed CO and OH is required to shift the equilibrium towards the carboxyl intermediate, which is achieved working at low H_2O/CO ratios. However, at P_{H2O}/P_{CO} = 90/10 Torr, CO coverage is so small that the TOF for carboxyl formation is four orders of magnitude lower than the value at P_{H2O}/P_{CO} = 10/90 Torr, with a concomitant lowering the overall H_2 TOF of the reaction. Finally, Fig. 6 reveals that the total percentage of CO_2 molecules formed through the surface redox route (*i.e.*, process 8) is slightly favoured at high P_{H2O}/P_{CO} ratios, since it is easier to find atomic oxygen produced from OH disproportionation. This increment in the

activity of the surface redox mechanism under an excess of water has been also observed by Stamatakis *et al*. for the WGSR on the Pt(111) and Pt(211) surfaces [41] .

4. Conclusions

In the present work, we report first-principles based kMC simulations of the WGSR on the stepped Cu(321) surface, including a total of 36 elementary steps such as adsorption/desorption, diffusion and other elementary surface chemical reactions, which allow to reach a clear picture of the overall reaction and to differentiate between surface redox and associative COOH mechanisms.

Reactions rates were obtained by combining transition state theory and collision theory. Diffusion reaction rates were scaled to speed up simulations but without affecting the final results. Recently published DFT results including dispersion were used for the computation of reaction rates at several temperatures. We consider a reliable lattice model for the Cu(321) surface, which allows discriminating different kind of sites: hollows, bridges and tops, which are involved in the most favourable elementary steps.

Temperature effects on WGSR were studied within the 463-625 K interval, showing a two-interval Arrhenius behaviour with apparent activation energies of 1.2 and 1.6 eV, much higher than the values observed for the Cu(111) surface (*i.e.*, 0.5-0.8 eV). The overall TOFs for the stepped Cu(321) surface were between two (at 625 K) and four (at 463 K) orders of magnitude lower than for the flat Cu(111) surface. Therefore, the stepped Cu(321) surface is catalytically less active than the Cu(111) one. This fact constitutes a new and unexpected conclusion, which possibly cannot be anticipated by inspection of the energy profiles of the WGSR only. This highlights the importance of performing macroscopic simulations, either using microkinetic models or kMC with the latter providing many additional details of the overall process.

Surface coverage effects were also analysed indicating that, for the WGSR on the Cu(321) surface, OH is the dominant adsorbed species and H the less important. Nevertheless, H_2O and H were the main adsorbed species at low temperatures, and both OH and H for higher temperatures for Cu(111).

Regarding the reaction mechanism, the associative COOH route is the dominant pathway in all the studied conditions like in the flat Cu(111) surface, but the surface redox route becomes also important at high temperatures, contributing around a 12% of the overall TOF. This effect was not observed in Cu(111) surface.

The determination of RDSs using the Capmbell's degree of rate control in kMC simulations, as in microkinetic modelling, seems to be accurate enough and coincident with the analysis of the frequencies of the surface processes.

The RDS at both temperatures appear to be the formation of CO_2 through the associative COOH route. This finding is not altered when reactants mixture composition is modified. Contrarily, water dissociation was the rate-determining step for Cu(111) surface.

As a closing remark, it is necessary to insist in the important results on the present work highlighting that the catalytic activity of stepped surfaces, and hence of low coordinated sites, is not always higher than that corresponding to terrace sites, even this type of sites exhibits higher adsorption energies for reactants and/or lower energy barriers for several forward processes (*e.g.*, for the possible RDSs) through the minimum energy reaction path. In fact, RDSs usually depend not only on the catalyst and P and T conditions but also on the surface coverages and on the details of the possible reverse processes. Therefore, only through kMC simulations or microkinetic modelling the RDSs can be unequivocally established.

Acknowledgments

Financial support to this research has been provided by the Spanish MINECO CTQ2014-53987-R and CTQ2015-64618-R grants and, in part, from the Generalitat de Catalunya grants 2014SGR97, 2014SGR1582 and XRQTC. This project received funding from the NOMAD Center of Excellence project from the European Union's Horizon 2020 research and innovation programme under grant agreement No 676580. HPG thanks Generalitat de Catalunya for a predoctoral FI-DGR-2015 grant and FI acknowledges additional support from the 2015 ICREA Academia Award for Excellence in University Research. Computational resources provided by *Consorci de Serveis Universitaris de Catalunya* (CSUC, former CESCA) are gratefully acknowledged.

Table 1. Elementary step characterization of the WGSR catalysed by the Cu(321) and Cu(111) surfaces: energy barriers ($E^0_{fwd,i}(0)$) and reaction energies ($\Delta E_i(0)$) at zero-coverage limit. Unless otherwise specified, species are adsorbed; label (g) is used for gas species. All values are in eV and include the ZPE correction.

		$E^0_{fwd,i}(0)$ **infinite separation (coadsorbed [17])**		$\Delta E_i(0)$ **infinite separation (coadsorbed [17])**	
ID	**elementary step**	**Cu(321)**	**Cu(111) [18]**	**Cu(321)**	**Cu(111) [18]**
1	$CO_{(g)} \leftrightarrow CO_{top1}$	0.00	0.00	-1.11	-0.51
2	$H_{2(g)} \leftarrow H_{2\ top1}$	-	-	-0.12	- [a]
3	$H_2O_{(g)} \leftrightarrow H_2O_{top1}$	0.00	0.00	-0.66	-0.18
4	$CO_{2(g)} \leftarrow CO_{2\ top1}$	-	-	-0.28	-0.09
5	$H_2O_{top1} \leftrightarrow OH_{b1-4}+H_{hole"b"}$	0.78 (0.78)	1.01	0.20 (0.18)	-0.14
6	$OH_{b1-2} \leftrightarrow O_{hole"a"}+H_{b1-4}$	1.61 (1.51)	1.60	0.48 (0.86)	0.41
7	$OH_{b1-2}+OH_{b1-3} \leftrightarrow H_2O_{top1}+O_{hole"b"}$	0.60 (0.46)	0.68	0.34 (-0.10)	0.68
8	$CO_{top1}+O_{hole"a"} \leftrightarrow CO_{2\ top1}$	0.68 (0.68)	0.79	-0.49 (-0.49)	-0.78
9	$CO_{top1}+OH_{hole"a"} \leftrightarrow c\text{-}COOH_{b1-2}$	0.86 (0.84)	0.70	0.62 (0.60)	0.15
10	$c\text{-}COOH_{b1-2} \leftrightarrow CO_{2\ top1}+H_{hole"a"}$	0.80 (0.80)	1.18	-0.55 (-0.52)	-0.51
11	$c\text{-}COOH_{b1-2}+OH_{b1-4} \leftrightarrow CO_{2\ top1}+H_2O_{top1}$	0.25 (0.33)	0.38	-0.77 (-0.63)	-0.37
12	$H_{hole"a"}+H_{hole"f"} \leftrightarrow H_{2\ top1}$	0.78 (0.78)	- [a]	0.31 (0.31)	- [a]
13	H diffusion (general)	-	0.15	-	0.00
13a	$H_{b1-4} \leftrightarrow H_{hole"a"}$	0.05	-	-0.28	-
13b	$H_{hole"a"} \leftrightarrow H_{hole"f"}$	0.20	-	0.15	-
13c	$H_{hole"f"} \leftrightarrow H_{b1-4}$	0.13	-	0.13	-
14	O diffusion (general)	-	0.38	-	0.00
14a	$O_{hole"a"} \leftrightarrow O_{hole"b"}$	0.44	-	0.00	-
15	OH diffusion (general)	-	0.12	-	0.12
15a	$OH_{b1-4} \leftrightarrow OH_{b1-3}$	0.11	-	0.06	-
15b	$OH_{b1-3} \leftrightarrow OH_{hole"a"}$	0.12	-	-0.30	-
15c	$OH_{hole"a"} \leftrightarrow OH_{b1-2}$	0.07	-	-0.05	-

[a] In the flat Cu(111) surface H_2 adsorption is dissociative (*i.e.*, $H_{2(g)} \leftrightarrow H+H$) [15,18]

Table 2. Campbell's degree of rate control ($X_{rc,\,i}$) for main candidates to be RDSs at two temperatures and three reactants mixtures.

		$X_{rc,\,i}$ [a]			
		625K P_{CO} = 26 Torr P_{H2O} = 10 Torr	500K P_{CO} = 26 Torr P_{H2O} = 10 Torr	625K P_{CO} = 10 Torr P_{H2O} = 90 Torr	625K P_{CO} = 90 Torr P_{H2O} = 10 Torr
5	$H_2O \leftrightarrow OH+H$	0.03	0.03	0.14	0.04
10	$c\text{-}COOH \leftrightarrow CO_2+H$	0.24	0.11	0.14	0.42
11	$c\text{-}COOH+OH \leftrightarrow CO_2+H_2O$	0.18	0.30	0.54	0.26
12	$H+H \leftrightarrow H_2$	0.03	0.00	0.05	0.18

[a] Campbell's degree of rate control [22] defines the degree at rate control for step i as

$$X_{rc,i} = \frac{k_i}{R}\frac{\delta R}{\delta k_i}$$

where R is the overall rate (i.e., H_2 TOF) and k_i the rate constant (r_i for kMC simulations). In the present study, changes of at least 10% in both r_i and r_{-i} were necessary to achieve significant and converged values. Moreover, diffusion rates were decreased to facilitate a faster although reliable calculation.

Fig. 1. Top view of the Cu(321) surface (left) and scheme of a 3×3 lattice model (right). Labels a, b, c, d, e and f refer to the hollow sites, whereas labels 1, 2, 3, 4 and 5 refer to the top sites. Grey lines in the lattice model represent the neighbouring connections between sites, and dotted red lines denote the 1×1 unit cell in.

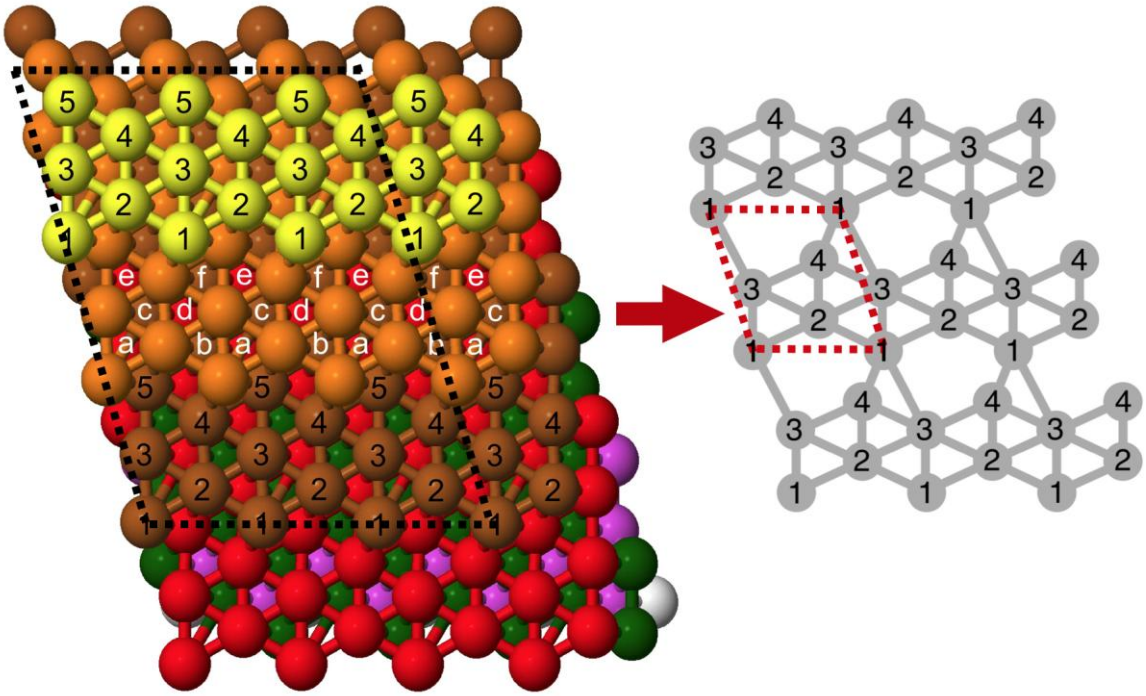

Fig. 2. Schematic representation of the process +10 in Table 1 (*i.e.*, *c*-$COOH_{b1\text{-}2}$ → $CO_{2\ top1}$ + $H_{hole"a"}$). Labels (*) and (**) are used for species occupying one or two top sites in the present lattice model, respectively.

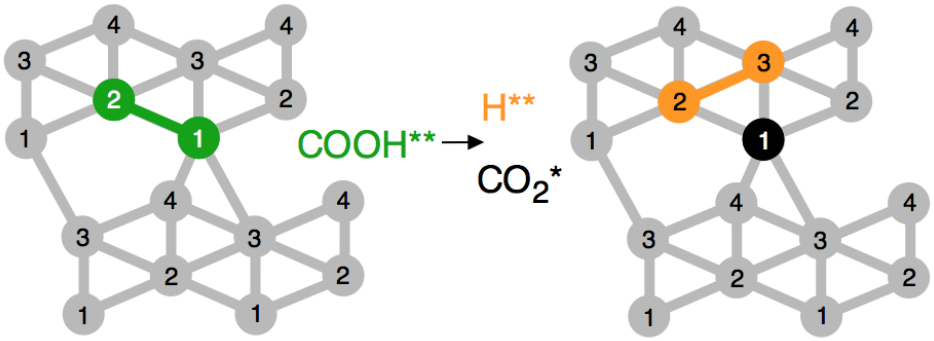

Fig. 3. Arrhenius plot of the WGSR on Cu(321) (red circles, this work) and on Cu(111) (blue squares, taken from Ref. 18) in the temperature range 463 – 625 K. Partial pressures of 26 and 10 Torr were used for CO and H_2O, respectively.

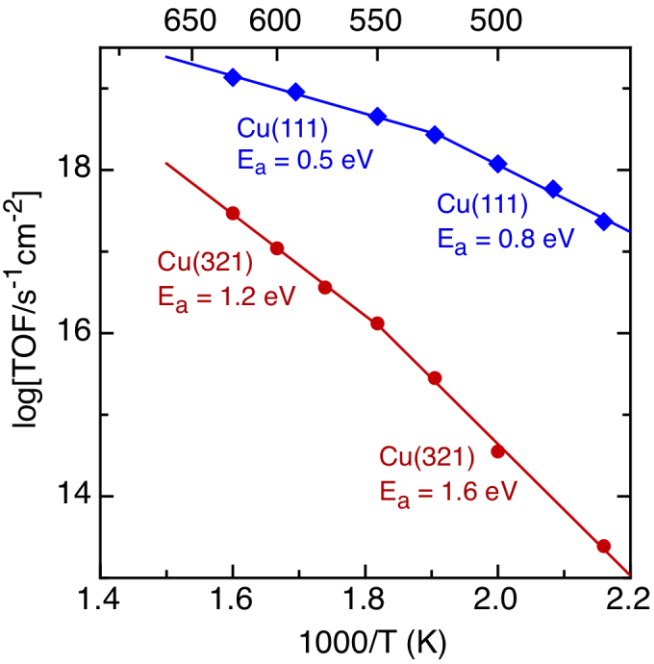

Fig. 4. Surface coverage for different adsorbates as a function of temperature for reactant partial pressures P_{CO} = 26 Torr and P_{H2O} = 10 Torr.

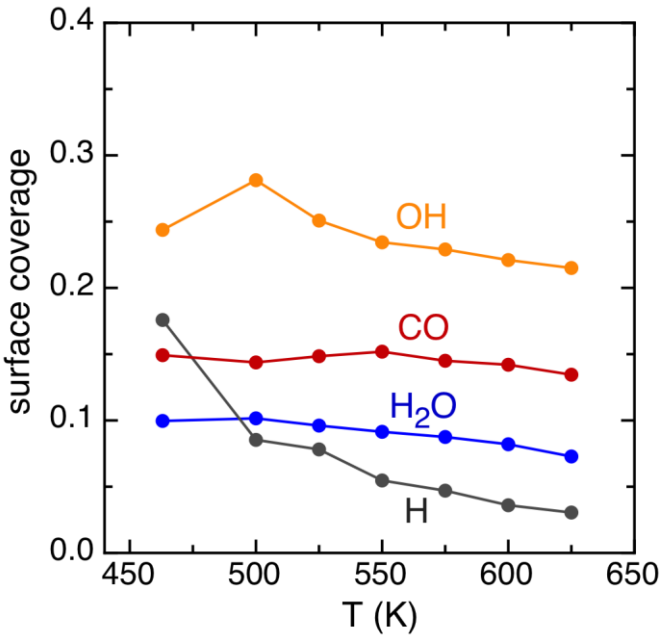

Fig. 5. (a) Relative contribution of each elementary step to the overall TOF as function of reaction temperature. Blue and green lines correspond to the associative COOH route, whereas red line corresponds to the surface redox route. (b) Frequencies of the main elementary processes at T = 500 K (left) and T = 625 K (right). Simulations performed at P_{CO} = 26 Torr and P_{H2O} = 10 Torr.

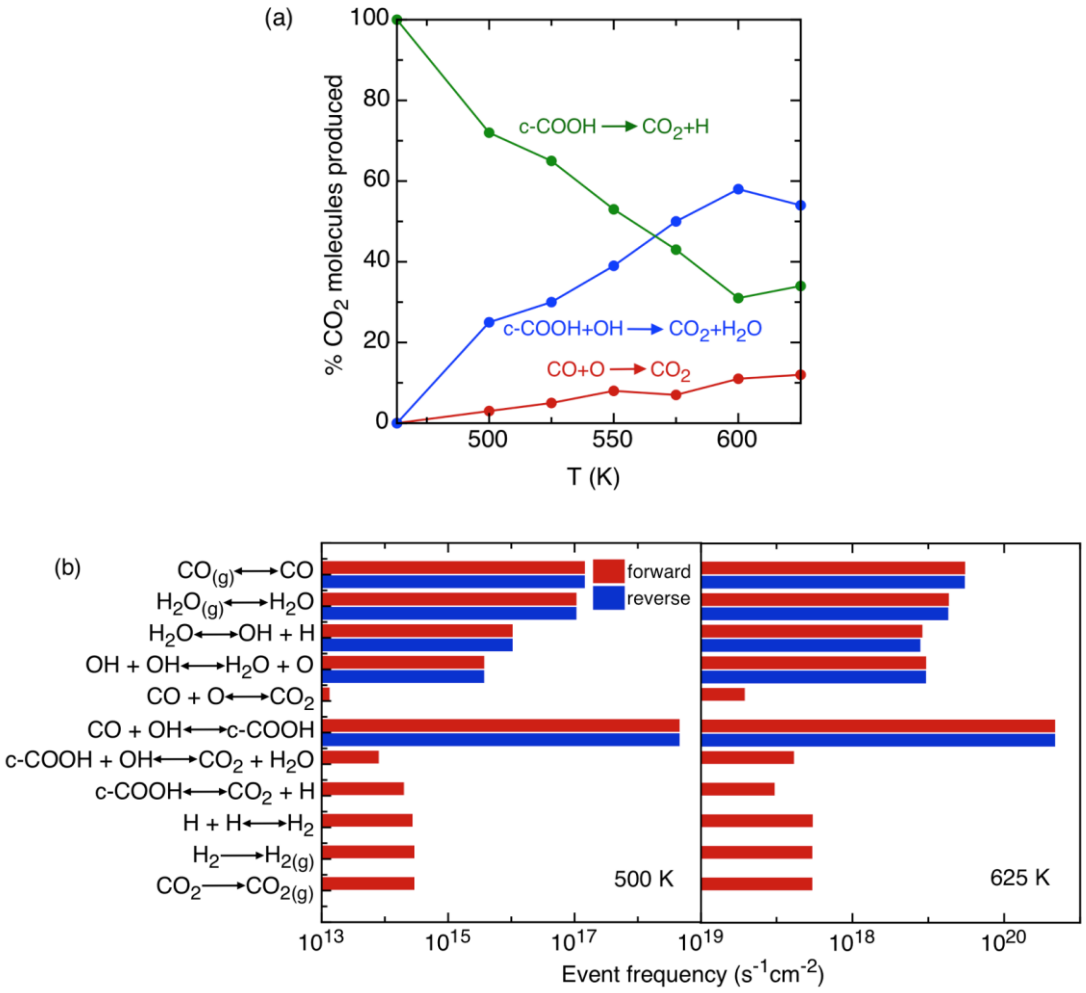

Fig. 6. (a) TOF (black line, squares) and surface coverage for different adsorbates (coloured lines, circles) as function of the reactant partial pressures for a constant total pressure of 100 Torr. (b) Frequencies of the main elementary processes for a total pressure of 100 Torr: P_{CO}/P_{H2O} equal to 10/90 (left) and 90/10 (right). All simulations were performed at T = 625 K.

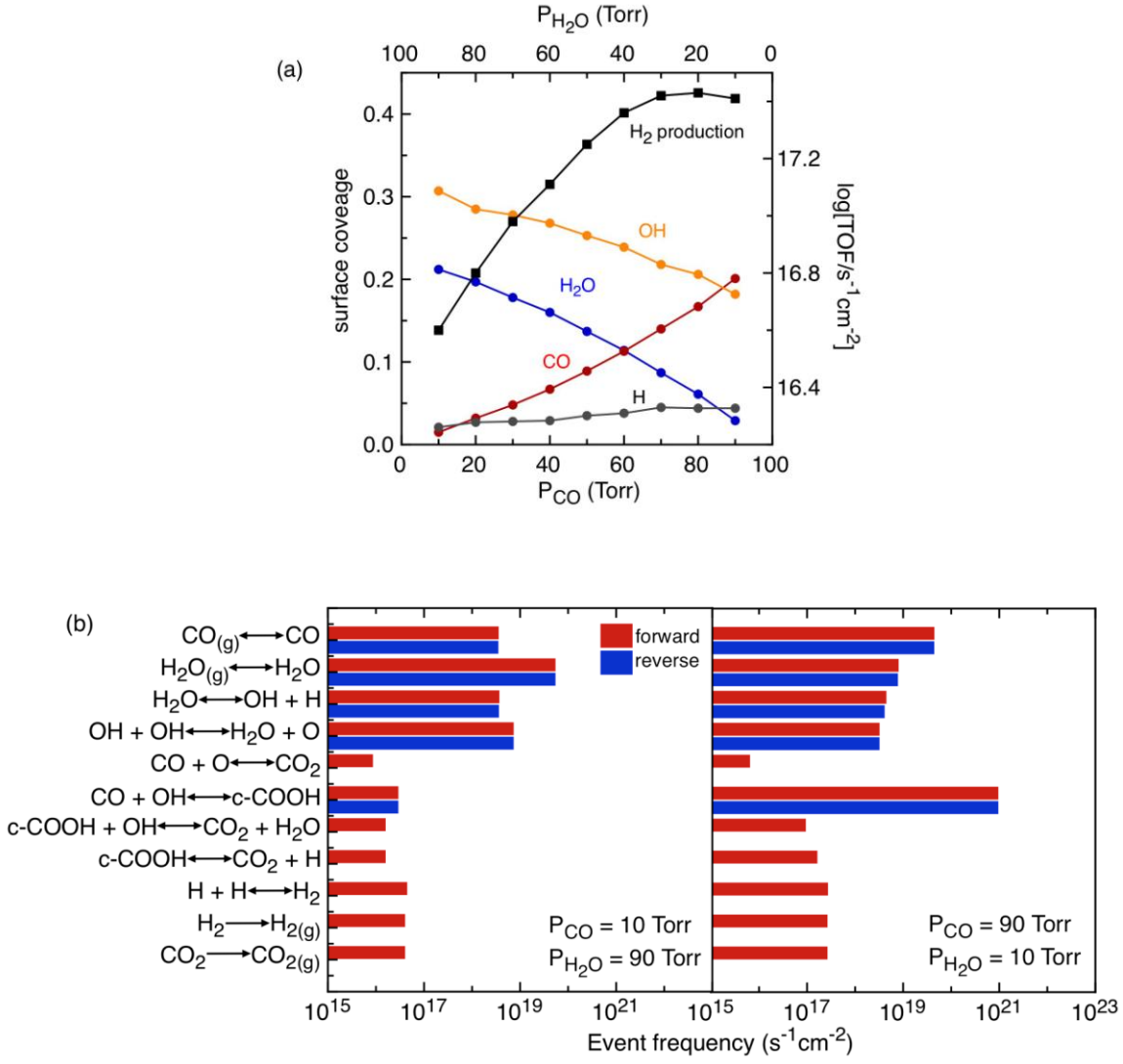

Graphical Abstract

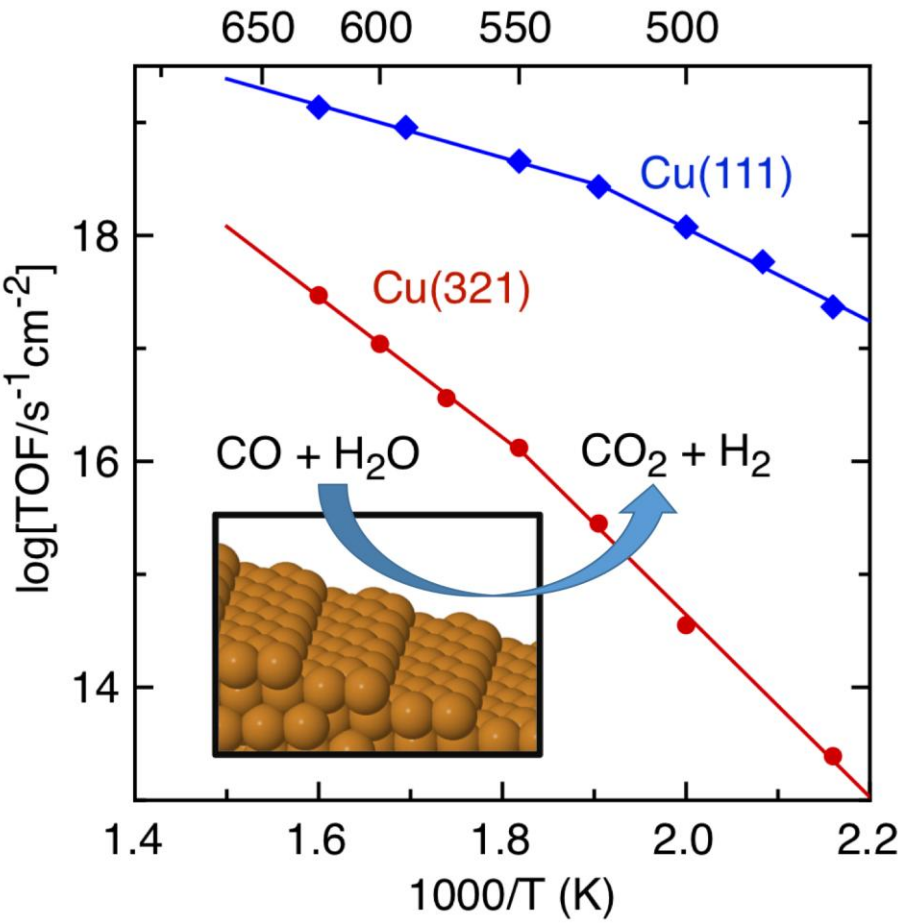

References

[1] J.T. Yates, Surface-chemistry at metallic step defect sites, J. Vac. Sci. Technol. A 13 (1995) 1359-1367.

[2] B.L.M. Hendriksen, M.D. Ackerman, R. van Rijn, D. Stoltz, I. Popa, O. Balmes, A. Resta, D. Wermeille, R. Felici, S. Ferrer, J.W.M. Frenken, The role of steps in surface catalysis and reaction oscillations, Nature Chem. 2 (2010) 730-734.

[3] J. Rostrup-Nielsen, J.K. Norskov, Step sites in syngas catalysis, Topics in Catal. 40 (2006) 45-48.

[4] B. Hammer, O.H. Nielsen, J.K. Norskov, Structure sensitivity in adsorption: CO interaction with stepped and reconstructed Pt surfaces, Catal. Lett. 46 (1997) 31-35.

[5] R.T. Vang, K. Honkala, S. Dahl, E.K. Vestergaard, J. Schnadt, E. Laegsgaard, B.S. Clausen, J.K. Norskov, F. Besenbacher, Controlling the catalytic bond-breaking selectivity of Ni surfaces by step blocking, Nat. Mater. 4 (2005) 160-162.

[6] K. Honkala, A. Hellman, I. N. Remediakis, A. Logadottir, A. Carlsson, S. Dahl, C. H. Christensen, J. K. Nørskov, Ammonia synthesis from first-principles calculations, Science, 307 (2005) 555-563.

[7] C.H. Bartholomew, Mechanisms of catalyst deactivation, App. Catal. A: General, 212 (2001) 17-60.

[8] D.S. Newsome, The Water-Gas Shift reaction, Catal. Rev.: Sci. Eng. 21 (1980) 275-318.

[9] D. Mendes, A. Mendes, L.M. Madeira, A. Iulianelli, J.M. Sousa, A. Basile, The water-gas shift reaction: from conventional catalytic systems to Pd-based membrane reactors – a review, Asia-Pac. J. Chem. Eng. 5 (2010) 111-137.

[10] D.W. Jeong, W.J. Jang, J.O. Shim, W.B. Han, H.S. Roh, U.H. Jung, W.L. Yoon, Low-temperature water-gas shift reaction over supported Cu catalysts, Renew. Energy, 65 (2014) 102-107.

[11] N.A. Koryabkina, A.A. Phatak, W.F. Ruettinger, R.J. Farrauto, F.H. Ribeiro, Determination of kinetic parameters for the water-gas shift reaction on copper catalysts under realistic conditions for fuel cell applications, J. Catal. 217 (2003) 233-239.

[12] D. Falleiros, F. Ademar, M. Kaminski, P. Matar, in: V. Patel (Ed.), Petrochemicals, Intech, Rijeka, Croatia, 2012 (Chapter 4).

[13] A. Bruix, J.A. Rodriguez, P.J. Ramírez, S.D. Senanayake, J. Evans, J.B. Park, D. Stacchiola, P. Liu, J. Hrbek, F. Illas, A new type of strong metal-support interaction and the production of H_2 through the transformation of water on $Pt/CeO_2(111)$ and $Pt/CeO_x/TiO_2(110)$ catalysts, J. Am. Chem. Soc., 134 (2012) 8968-8974.

[14] J.A. Rodriguez, P.J. Ramírez, G.G. Asara, F. Viñes, J. Evans, P. Liu, J.M. Ricart, F. Illas, Charge polarization at a Au-TiC interface and the generation of highly active and selective catalysts for the low-temperature water-gas shift reaction, Angew. Chem., Int. Ed., 53 (2014) 11270-11274.

[15] A.A. Gokhale, J.A. Dumestic, M. Mavrikakis, On the mechanism of low-temperature water gas shift reaction on copper, J. Am. Chem. Soc. 130 (2008) 1402-1414.

[16] J.L.C. Fajín, M.N.D.S. Cordeiro, F. Illas, J.R.B. Gomes, Influence of step sites in the molecular mechanism of the water gas shift reaction catalysed by copper, J. Catal., 268 (2009) 131-141.

[17] H. Prats, P. Gamallo, R. Sayós, F. Illas, Unexpectedly large impact of van der Waals interactions on the description of heterogeneously catalysed reactions: the water gas shift reaction Cu(321) as a case example, Phys. Chem. Chem. Phys., 18 (2016) 2792-2801.

[18] H. Prats, L. Álvarez, F. Illas, R. Sayós. Kinetic Monte Carlo simulations of the water gas shift reaction on Cu(111) from density functional theory based calculations, J. Catal. 333 (2016) 217-226.

[19] G. Wang, L. Jiang, X. Pang, Z. Cai, Y. Pan, X. Zhao, Y. Morikawa, J. Nakamura, A theoretical study of surface-structural sensitivity of the reverse water-gas shift reaction over Cu(hkl) surfaces, Suf. Sci. 543 (2003) 118-130.

[20] G. Wang, L. Jiang, Z. Cai, Y. Pan, X. Zhao, W. Huang, K. Xie, Y. Li, Y. Sun, B. Zhong, Surface structure sensitivity of the water-gas shift reaction on Cu(hkl) surfaces: A theoretical study, J. Phys. Chem. B, 107 (2003) 557-562.

[21] C.A. Callaghan, in *Kinetics and Catalysis of the Water-Gas-Shift Reaction: A Microkinetic and Graph Theoretic Approach*, Doctoral Thesis, Worcester Polytechnic Institute, 2006.

[22] C.T. Campbell, Micro- and macro-kinetics: their relationship in heterogeneous catalysis, Topics Catal. 1 (1994) 353-366.

[23] C.A. Callaghan, S.A. Vilekar, I. Fishtik, R. Datta, Topological analysis of catalytic reaction networks: Water gas shift reaction on Cu(111), Appl. Catal. A: General, 345 (2008) 213-232.

[24] J.A. Dumesic, Analyses of reaction schemes using De Donder Relations, J. Cat. 185 (1999) 496-505.

[25] Stegelmann, A. Andreasen, C. T. Campbell, Degree of rate control: how much the energies of intermediates and transition states control rates, J. Amer. Chem. Soc. 131 (2009) 8077-8082.

[26] H. Meskine, S. Matera, M. Scheffler, K. Reuter, H. Metiu, Examination of the concept of degree of rate control by first-principles kinetic Monte Carlo Simulations, Surf. Sci. 603 (2009) 1724-1730.

[27] G. Kresse, J. Hafner, Ab initio olecular dynamics for liquid metals, Phys. Rev. B: Condens. Matter Mater. Phys. 47 (1993) 558-561.

[28] G. Kresse, J. Furthmüller, Efficiency of ab-initio total energy calculations for metals and semiconductors using a plane-wave basis set, Condens. Comput. Mater. Sci. 6 (1996) 15-50.

[29] G. Kresse, J. Furthmüller, Efficient iterative schemes for ab initio total-energy calculations using a plane-wave basis set, J. Phys. Rev. B: Condens. Matter Mater. Phys. 54 (1996) 11169-11186.

[30] D. R. Lide, CRC Handbook of Chemistry and Physics. Ed. Lide, D. R.; CRC Press, Boca Raton, USA, 88th edn, 2008.

[31] J. P. Perdew, K. Burke, M. Ernzerhof, Generalized gradient approximation made simple, Phys. Rev. Lett. 77, (1996) 3865-3868.

[32] S. Grimme, Semiempirical GGA-type density functional constructed with a long-range dispersion correction, J. Comput. Chem. 27 (2006) 1787-1799.

[33] P. E. Blöchl, Projector augmented-wave method, Phys. Rev. B: Condens. Matter Mater. Phys. 50, (1994) 17953-17979.

[34] G. Kresse, D. Joubert, From ultrasoft pseudopotentials to the projector augmented-wave method, Phys. Rev. B: Condens. Matter Mater. Phys. 59 (1999) 1758-1775.

[35] H. J. Monkhorst, J. D. Pack, Special points for Brillouin-zone integrations, Phys. Rev. B: Condens. Matter Mater. Phys. 13 (1976) 5188-5192.

[36] M. Stamatakis, Kinetic modelling of heterogeneous catalytic systems, J. Phys. Condens. Matter. 27 (2015) 013001:1-28.

[37] M. Stamatakis, D.G. Vlachos, A graph-theoretical kinetic Monte Carlo framework for on-lattice chemical kinetics, J. Chem. Phys. 134 (2011) 214115:1-13.

[38] J. Nielsen, M. d'Avezac, J. Hetherington, M. Stamatakis, Parallel kinetic monte Carlo simulation framework incorporating accurate models of adsorbate lateral interactions, J. Chem. Phys. 2013, 139, 224706:1-13.

[39] M. Stamatakis, D.G. Vlachos, Unravelling the complexity of catalytic reactions via kinetic Monte Carlo simulation: current status and frontiers, ACS Catal. 2 (2012) 2648-2663.

[40] A.P.J. Jansen, An introduction to kinetic Monte Carlo simulations of surface reactions, Lecture Notes in Physics, vol. 856, Springer-Verlag, Heidelberg, Germany, 2012.

[41] M. Stamatakis, Y. Chen, D.G. Vlachos, First-principles-based kinetic Monte Carlo simulation of the structure sensitivity of the water-gas shift reaction on platinum surfaces, J. Phys. Chem. C. 115 (2011) 24750-24762.

[42] K. J. Laidler, Chemical Kinetics, Harper & Row Publishers, New York, USA, 1987.

[43] D. A. McQuarrie, Statistical Mechanics, 2nd ed.; Harper & Row, New York, 2000.

[44] H. Tang, A. Van der Ven, B.L. Trout, Phae diagram of oxygen adsorbed on platinum (111) by first-principles investigation, Phys. Rev. B 70 (2004) 045420:1-10.

[45] B.C. Han, A. Van der Ven, G. Ceder, B Hwang, Surface segregation and ordering of alloy surfaces in the presence of adsorbates, J. Phys. Rev. B 72 (2005) 205409:1-9.

[46] S.D. Miller, J.R. Kitchin, Uncertainty and figure selection for DFT based cluster expansions for oxygen adsorption on Au and Pt(111) surfaces, Mol. Simul. 35 (2009) 920-927.

[47] D. Lerch, O. Wieckhorst, G. Hart, R. Forcade, S. Müller, UNCLE: a code for constructing cluster expansions for arbitrary lattices with minimal user-input, Modell. Simul. Mater. Sci. Eng. 17 (2009) 055003:1-19.

[48] C. Wu, D.J. Schmidt, C. Wolverton, W.F. Schneider, Accurate coverage-dependence incorporated into first-principles kinetic models: Catalytic NO oxidation on Pt(111), J. Catal. 286 (2012) 88-94.

[49] R.B. Getman, W.F. Schneider, DFT-based coverage-dependent model of Pt-catalyzed NO oxidation, Chem. Cat. Chem. 2 (2010) 1450-1460.

[50] J.K. Nørskov, T. Bligaard, A. Logadottir, S. Bahn, L.B. Hansen, M. Bollinger, H. Bengaard, B. Hammer, Z. Sljivancanin, M. Mavrikakis, Y. Xu, S. Dahl, J.H. Jacobsen, Universality in heterogeneous catalysis, J. Catal. 209 (2002) 275-278.

[51] L.C. Grabow, A.A. Gokhale, S.T. Evans, J.A. Dumestic, M. Mavrikakis, Mechanism of the water gas shift reaction on Pt: first principles, experiments, and microkinetic modelling, J. Phys. Chem. C 112 (2008) 4608-4617.

[52] S. Piccinin, M. Stamatakis, CO oxidation on Pd(111): a first-principles-based kinetic Monte Carlo study, ACS Catal. 4 (2014) 2143-2152.

[53] I. Bönicke, W. Kirstein, S. Spinzig, F. Thieme, CO adsorption studies on a stepped Cu(111) surface, Surf. Sci. 313 (1994) 231-238.

[54] B.J. Hinch, L.H. Dubois, Water adsorption on Cu(111): evidence for Volmer-Weber film growth, Chem. Phys. Lett. 181 (1991) 10-15.

[55] L. Yang, A. Karim, J.T. Muckerman, Density functional kinetic Monte Carlo simulation of water-gas shift reaction on Cu/ZnO, J. Phys. Chem. C, 117 (2013) 3414-3425.

[56] M. Stamatakis, D.G. Vlachos, Equivalence of on-lattice stochastic chemical kinetics with the well-mixed chemical master equation in the limit of fast diffusion, Comput. Chem. Eng. 35 (2012) 2602-2610.

[57] Y.C. Huang, T. Zhou, C. Ling, S. Wang, J.Y. Du, Do Ni/Cu and Cu/Ni alloys have different catalytic performances towards water-gas shift? A density functional theory investigation, ChemPhysChem 15 (2014) 2490-2496.

[58] S.-C. Huang, C.-H. Lin, J.-H. Wang, Trends of water gas shift reaction on close-packed transition metal surfaces, J. Phys. Chem. C 114 (2010) 9826-9834.